JOURNAL OF AIRCRAFT
Vol. 44, No. 1, January–February 2007

Volterra Kernel Extrapolation for Modeling Nonlinear Aeroelastic Systems at Novel Flight Conditions

Richard J. Prazenica*
University of Florida, Shalimar, Florida 32579
Patrick H. Reisenthel†
Nielsen Engineering and Research, Inc., Mountain View, California 94043-2241
Andrew J. Kurdila‡
Virginia Polytechnic Institute and State University, Blacksburg, Virginia 24061
and
Martin J. Brenner§
NASA Dryden Flight Research Center, Edwards, California 93523-0273

DOI: 10.2514/1.22764

This paper investigates the modeling of parameter-varying nonlinear aeroelastic systems using Volterra theory. With this approach, the system dynamics are expressed in terms of a set of Volterra kernels. It is well known that the parameters of aeroelastic systems, such as natural frequencies and damping ratios, change with flight condition. Therefore, a system is characterized by a different set of Volterra kernels at each flight condition. These kernels must be extracted from the flight data at each flight condition of interest: a relatively costly procedure. This paper presents a kernel extrapolation method designed to model first- and second-order kernels as functions of a single varying parameter, such as altitude or Mach number. First, using a multiwavelet-based algorithm, a set of Volterra kernels is identified from the input/output data at a number of flight conditions. In this manner, each kernel is represented in terms of a set of multiwavelet basis functions. An extrapolation model is then obtained by using a polynomial curve-fit to express the magnitude of each basis coefficient as a function of the varying parameter. The performance of this kernel extrapolation method is studied in detail for a simulated nonlinear aeroelastic system, demonstrating the validity of the approach. Then, the algorithm is applied to flight data from the F/A-18 Active Aeroelastic Wing. This example illustrates some of the difficulties associated with extrapolating kernels from noisy flight data.

Introduction

NONLINEAR aeroelasticity has been an active research field in recent years [1,2]. A wide variety of methods have been applied to the study of nonlinear aeroelastic systems including describing functions [3], higher-order spectra [4,5], artificial neural networks [6], harmonic balance [7], nonlinear autoregressive moving-average with exogenous input (NARMAX) models [8], the reverse-path spectral method [9], and the Hilbert–Huang transform [10]. This paper focuses on the Volterra series, which has proven to be a useful tool for the analysis of nonlinear aeroelastic systems [11–17]. With this approach, a given system is modeled in terms of a set of Volterra kernels which characterize dynamics of varying order. In particular, the first-order kernel represents the linear dynamics of the system whereas higher-order kernels model the nonlinear dynamics. These kernels, which must be identified from measured experimental data, can provide useful information such as whether or not an aircraft is close to flutter. A drawback in applying Volterra models to aeroelastic systems, however, is that the kernels are parametrically dependent on flight condition (e.g., altitude and Mach number). This is a direct consequence of the fact that aeroelastic systems evolve with changing flight conditions. Therefore, to represent the dynamics of an aeroelastic system, a different set of Volterra kernels must be identified at each flight condition. Given that kernel identification is not a trivial task, it would be beneficial to be able to model the evolution of the kernels as a function of flight condition. In addition, such a capability would have the potential to minimize the number of flight test points needed for flutter clearance, as an example.

Parameter-varying Volterra kernels have been explored for predicting the onset of linear flutter [18]. In the study presented in [18], parameter-varying first-order kernels were employed to account for unmodeled (i.e., incorrectly modeled) linear dynamics in a robust stability framework. It was demonstrated that this approach could be used to successfully predict the linear flutter speed of a simulated pitch-plunge aeroelastic system. This current paper investigates the extrapolation of first- and second-order Volterra kernels to model nonlinear aeroelastic systems at novel flight conditions. First, a multiwavelet-based kernel identification algorithm [19] is used to extract kernels from measured input/output data over a set of flight conditions. In this manner, each kernel is represented as a linear combination of multiwavelet basis functions. The extrapolation procedure then entails using a polynomial curve-fit to express each basis coefficient as a function of a single varying parameter, such as velocity, altitude, or Mach number. With this approach, then, a model is obtained that yields estimates of the kernels at any value of the parameter. As would be expected, the quality of these predictions deteriorates as the kernels are extrapolated further away from the test points used for the curve-fit.

The kernel extrapolation method is first applied to simulated data from a prototypical aeroelastic system under noise-free conditions.

Presented as Paper 1939 at the 45th AIAA Structures, Structural Dynamics, and Materials Conference and Exhibit, Palm Springs, CA, 19–22 April 2004; received 26 January 2006; revision received 4 August 2006; accepted for publication 10 August 2006. Copyright © 2006 by Richard J. Prazenica. Published by the American Institute of Aeronautics and Astronautics, Inc., with permission. Copies of this paper may be made for personal or internal use, on condition that the copier pay the $10.00 per-copy fee to the Copyright Clearance Center, Inc., 222 Rosewood Drive, Danvers, MA 01923; include the code $10.00 in correspondence with the CCC.

*Visiting Assistant Professor, Research in Engineering Education Facility (UF-REEF), 1350 North Poquito Road; prazenic@ufl.edu. Member AIAA.
†Chief Scientist, 605 Ellis Street, Suite 200; phr@nearinc.com. Senior Member AIAA.
‡W. Martin Johnson Professor, Department of Mechanical Engineering, 100S Randolph Hall; kurdila@vt.edu. Associate Fellow AIAA.
§Aerospace Engineer, Aerostructures Branch, Structural Dynamics Group, P.O. Box 273, MS 4840D; martin.j.brenner@nasa.gov.

This example serves to validate the approach for first- and second-order Volterra kernels. Then, the method is applied to the more challenging case of flight data from the F/A-18 Active Aeroelastic Wing (AAW). It should be emphasized that this example differs significantly from the noise-free analytical system in that the identification of Volterra kernels is a far more challenging task. Nevertheless, in previous work, the multiwavelet-based algorithm has been successfully employed to identify first-, second-, and third-order kernels from AAW flight data [15]. The identified kernels are relatively noisy, a reflection of the noisy characteristics of the flight data. The results given in this paper show that, whereas kernel extrapolation is possible, using kernels identified from noisy flight data limits the range over which first- and second-order kernels can effectively be extrapolated.

Volterra Kernel Identification

Volterra series representations provide a convenient framework for the analysis of nonlinear dynamic systems. The Volterra theory of nonlinear systems states that the system output y can be expressed in terms of an infinite series of integral operators of increasing order [20,21]. In practice, the series is truncated and this paper considers Volterra models that include only the first- and second-order operators. For a causal, time-invariant, single-input/single-output system, these operators take the form

$$y_1(t) = \int_0^t h_1(\xi)u(t-\xi)\,\mathrm{d}\xi \tag{1}$$

$$y_2(t) = \int_0^t \int_0^t h_2(\xi,\eta)u(t-\xi)u(t-\eta)\,\mathrm{d}\xi\,\mathrm{d}\eta \tag{2}$$

where u is the input and h_1, h_2 are the first- and second-order Volterra kernels. Collectively, the Volterra kernels provide a model of the system because, once the kernels have been successfully identified, the response to any arbitrary input can be determined. The first-order kernel represents the linear dynamics of the system whereas the kernels of second-order and higher characterize the nonlinear dynamics. It should be noted that, for a linear system, the first-order kernel is equivalent to the impulse response of the system and the output is given by Eq. (1). Therefore, the Volterra theory can be viewed as an extension of the concept of linear convolution to nonlinear systems.

It has been demonstrated that Volterra models are applicable to a large class of dynamic systems, including aeroelastic systems. In using such models, the problem of system identification is equivalent to identifying the Volterra kernels of a given system. A diverse range of approaches have been taken to kernel identification in both the time and frequency domains. These include direct measurement techniques such as harmonic probing [13,22] and the application of discrete impulse inputs [12,23], statistical approaches such as the cross-correlation technique [24], and the expansion of the kernels in terms of a set of basis functions [14,25].

This paper employs a multiwavelet-based kernel identification algorithm in which orthonormal, piecewise-polynomial multiwavelets are used to approximate first- and second-order Volterra kernels. This algorithm has been thoroughly described in a recent paper [19] and is only briefly reviewed here. Basically, wavelets are compactly supported, oscillatory functions that are constructed to satisfy certain properties such as orthogonality, smoothness, and symmetry requirements [26]. Multiwavelets compose a set of wavelet functions $\{\psi^1,\ldots,\psi^r\}$ that are generated from a set of scaling functions $\{\phi^1,\ldots,\phi^r\}$ [27]. The scaled translates and dilates of the multiwavelets form a basis for $L^2(\mathbb{R})$, the space of square-integrable functions. The motivation for the multiwavelet-based approach is that wavelets provide time and frequency localization of functions or signals. Often, many of the wavelet coefficients are close to zero and can be neglected, leading to reduced-order representations of the kernels.

For the purposes of this paper, which focuses on kernel extrapolation, the multiwavelet expansions of the first- and second-order kernels can be simply written as

$$h_1(\xi) = \sum_{j=1}^{N_1} c_{1,j} f_{1,j}(\xi) \tag{3}$$

$$h_2(\xi,\eta) = \sum_{j=1}^{N_2} c_{2,j} f_{2,j}(\xi,\eta) \tag{4}$$

Although the specific algorithm employed in this paper uses multiwavelet basis functions, $\{f_{1,j}\}_{j=1}^{N_1}$ and $\{f_{2,j}\}_{j=1}^{N_2}$ can be considered as any set of one- and two-dimensional basis functions. Once the kernels have been expressed in terms of a set of basis functions, a matrix formulation is obtained in which a least-squares problem must be solved for the basis coefficients that represent the kernels. This is fundamentally an ill-posed, inverse problem for which the solution is sensitive to noise in the data, especially as the number of model coefficients is increased. Therefore, it is critical to use a regularization technique, such as the truncated singular value decomposition, to solve the least-squares problem.

Kernel Extrapolation Procedure

This paper considers a simple approach to kernel extrapolation designed to model the evolution of each basis function coefficient in the kernel representations as a function of a single varying parameter. First, a set of kernels is identified from the data at a number of different values of the parameter. Then, a polynomial curve-fit is performed for each basis coefficient, expressing each coefficient as a function of the varying parameter. In this manner, a model is obtained to predict the kernels at any given value of the parameter. In this paper, this approach is applied for the extrapolation of first- and second-order kernels, but the method can easily be extended to higher-order kernels.

There are many possible variations of this approach to kernel extrapolation. The number of identified kernels used to perform the curve-fit is one variable to be chosen. Similarly, the degree of the polynomial used for the curve-fit must also be selected. Another possible variation on this approach, which resembles what might be done during a flight test, is to first perform an initial curve-fit based on a set of identified kernels. Then, kernels could be extrapolated until the predicted kernels exceed a given error bound. At that point, a new kernel would need to be identified from measured input/output data (i.e., a new flight test point would be required). A new curve-fit, incorporating the newly identified kernel, would then be performed and used to extrapolate more kernels. This procedure could be repeated as necessary. In taking this approach, one would need to choose between a "global" curve-fit that uses the full set of identified kernels and a "local" fit that uses only a certain number of recently identified kernels to compute the extrapolation model.

The extrapolation procedure is best introduced in the context of an example. In this section, the approach is validated on a simulated pitch-plunge aeroelastic system. Then, in the following section, the feasibility of kernel extrapolation for the F/A-18 Active Aeroelastic Wing (AAW) is considered.

Pitch-Plunge Aeroelastic System

The pitch-plunge system considered in this section models an experimental apparatus that was constructed at Texas A&M University to study limit cycle oscillation (LCO). The experimental setup consists of an airfoil section with a trailing-edge flap for control actuation. This system, which has been studied extensively in the literature, can be modeled by a pair of coupled second-order differential equations:

Table 1 Parameters for the pitch-plunge aeroelastic system

$m = 12.387$ kg	$a = -0.6$	$c_{l_\alpha} = 6.28$	$k_h = 2844.4$ N/m
$I_\alpha = 0.065$ m$^2 \cdot$ kg	$x_\alpha = 0.2466$	$c_{m_\alpha} = -0.628$	$k_{\alpha_1} = 2.82$ N $\cdot$ m
$\rho = 1.225$ kg/m^3	$c_h = 27.43$ kg/s	$c_{l_\beta} = 3.358$	$k_{\alpha_2} = 14.1$ N $\cdot$ m
$b = 0.135$ m	$c_\alpha = 0.180$ m$^2 \cdot$ kg/s	$c_{m_\beta} = -0.635$	

$$\begin{bmatrix} m & mx_\alpha b \\ mx_\alpha b & I_\alpha \end{bmatrix} \begin{Bmatrix} \ddot{h} \\ \ddot{\alpha} \end{Bmatrix} + \begin{bmatrix} c_h & 0 \\ 0 & c_\alpha \end{bmatrix} \begin{Bmatrix} \dot{h} \\ \dot{\alpha} \end{Bmatrix} + \begin{bmatrix} k_h & 0 \\ 0 & k_\alpha(\alpha) \end{bmatrix} \begin{Bmatrix} h \\ \alpha \end{Bmatrix} = \rho U^2 b \begin{bmatrix} c_{l_\alpha}\left(\alpha + \frac{1}{U}\dot{h} + \frac{1}{U}\left(\frac{1}{2} - a\right)b\dot{\alpha}\right) \\ c_{m_\alpha}\left(b\alpha + \frac{1}{U}b\dot{h} + \frac{1}{U}\left(\frac{1}{2} - a\right)b^2\dot{\alpha}\right) \end{bmatrix} + \rho U^2 b \begin{bmatrix} -c_{l_\beta} \\ c_{m_\beta} b \end{bmatrix} \beta \tag{5}$$

where h denotes the plunge displacement of the airfoil and α represents the pitch angle. The terms on the left-hand side of Eq. (5) describe the structural dynamics of the system whereas the terms on the right-hand side represent quasi-steady aerodynamic forces and moments. The outputs of the system are the pitch angle and the plunge displacement. The input is given by the angular deflection β of the trailing-edge flap. It should be noted that, because the system has two outputs, there are two sets of Volterra kernels that characterize the system: one for the pitch angle and the other for the plunge response. Because there is only one input, the pitch and plunge kernels can be identified by considering two separate single-input/single-output systems.

The values of the various system parameters are listed in Table 1. The pitch-plunge system is nonlinear due to a polynomial torsional spring stiffness $k_\alpha(\alpha)$. In this example, the stiffness polynomial is chosen as

$$k_\alpha(\alpha) = k_{\alpha_1} + k_{\alpha_2}\alpha \tag{6}$$

so that the restoring moment is a quadratic function of the pitch angle. Whereas other studies have considered polynomial stiffness functions of up to fourth order, the simpler stiffness function in Eq. (6) has been chosen here to emphasize the contribution of the second-order Volterra kernel to the nonlinear response. It should be noted that, although the torsional stiffness is a quadratic function of the pitch angle, the nonlinearity is not completely characterized by the second-order kernel. For relatively small-amplitude input excitations (i.e., on the order of 5 deg or less), however, the contribution of the second-order kernel tends to dominate the nonlinear response. If the torsional stiffness were an odd function of the pitch angle, then the system would be characterized in terms of only the odd-ordered kernels and the second-order kernel would be zero.

The equations of motion of the pitch-plunge system have been simulated using fourth-order Runge–Kutta numerical integration with a variable step size. In this study, the flow velocity is varied to study the evolution of the first- and second-order kernels as a function of a single parameter. The underlying linear system, obtained by setting $k_{\alpha_2} = 0$ in Eq. (6), becomes unstable when the flow velocity reaches 12.4 m/s. This results from a classical flutter mechanism in which the natural frequencies of the system coalesce near the flutter speed. As this occurs, the damping of the plunge mode increases while the damping of the pitch mode decreases. When the linear flutter speed is reached, the damping of the pitch mode changes sign, resulting in unstable oscillation. The behavior of the nonlinear system is different, however. As the flow velocity approaches the linear flutter speed, the nonlinear torsional stiffness term drives the system into a limit cycle, characterized by bounded periodic motion. The unforced response of the linear and nonlinear aeroelastic systems to an initial pitch angle of 5.73 deg at the linear flutter speed is depicted in Fig. 1. The linear pitch and plunge responses clearly increase monotonically while the nonlinear responses converge to limit cycles.

First-Order Kernel Extrapolation

First-order kernels were identified from simulated input/output data from the linear pitch-plunge system over the following set of flow velocities:

$$U = \{0.1, 0.5, 1.0, 1.5, 2.0, 2.5, 3.0, 3.5, 4.0, 4.5, 5.0, 5.5, 6.0, 6.5, 7.0, 7.5, 8.0, 8.25, 8.5, 8.75, 9.0, 9.25, 9.5, 9.75, 10.0, 10.1, 10.2, 10.3, 10.4, 10.5, 10.6, 10.7, 10.8, 10.9, 11.0, 11.1, 11.2, 11.3, 11.4, 11.5, 11.6, 11.7, 11.8, 11.9, 12.0, 12.1, 12.2, 12.3, 12.4, 12.5\} \text{ m/s}$$

The underlying linear system becomes unstable at a flow velocity of approximately 12.4 m/s. As the velocity approaches this value, the kernels tend to change more rapidly with increasing velocity. Therefore, the kernels were measured at smaller increments in U to reflect this characteristic. In the extrapolation procedure, a subset of these measured kernels is used to perform the curve-fit. The remaining kernels in the set are used to evaluate the accuracy of the extrapolated kernels.

Two sets of kernels were identified, one corresponding to the pitch angle and the other corresponding to the plunge. The kernels were identified using the multiwavelet-based algorithm that was described earlier. Because the kernel extrapolation procedure requires the curve-fitting of the kernel basis coefficients, it was necessary to express each kernel in terms of the same set of multiwavelets. Each

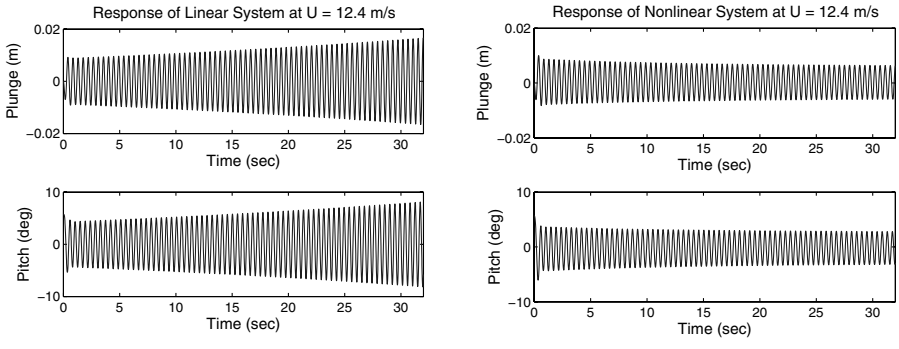

Fig. 1 Unforced pitch and plunge responses at the linear flutter speed.

first-order kernel was represented in terms of 257 multiwavelet basis functions over an 8 s time interval. In each case, only 8 s of input/output data from a simple step input, sampled at a rate of 128 Hz, were needed to accurately identify the kernels in that time interval. For almost all values of the flow velocity, the kernels decay to zero within 8 s. As the flow velocity approaches the instability at 12.4 m/s, however, the kernels no longer decay to zero within the 8 s time interval.

First-order kernels have been extrapolated from the polynomial models of the basis coefficients and compared with the actual measured kernels. A measure of error for each extrapolated first-order kernel can be defined in terms of the rms error as

$$E_1 = \frac{\{\sum_{i=1}^{p_1}[h_1(i) - \hat{h}_1(i)]^2\}^{1/2}}{[\sum_{i=1}^{p_1} h_1(i)^2]^{1/2}} \tag{7}$$

where h_1 denotes the actual measured kernel and $\hat{h}_1$ represents the extrapolated kernel. Each kernel is plotted in terms of $p_1 = 1025$ discrete points, and these discrete kernel values are used to compute the error measure. Here, it should be noted that the measured kernels are taken as the true kernels for the purposes of error estimation. Because these kernels were identified from simulated linear, noise-free data, this is a reasonable approximation.

One-Time Curve-Fit and First-Order Kernel Extrapolation

This example considers the extrapolation of first-order pitch kernels using the kernels identified at the following six flow velocities:

$$U_{\text{fit}} = \{3.0, 3.5, 4.0, 4.5, 5.0, 5.5\} \text{ m/s}$$

Polynomial curve-fits have been performed for each of the 257 basis coefficients as they vary across these six flow velocities. As a result, each basis coefficient is modeled as a polynomial function of flow velocity. This model enables the prediction of each basis coefficient at any given flow velocity and, consequently, yields a prediction of the first-order kernel.

One variable in the kernel extrapolation procedure is the degree of the polynomial chosen for the curve-fit. Figure 2 plots the error in the extrapolated pitch kernels as a function of flow velocity for different polynomial fits. In this example, linear, quadratic, cubic, fourth-order, and fifth-order fits were performed. Each polynomial fit was obtained by solving a least-squares problem for each polynomial coefficient. Note that, because six data points were used to form the model, the fifth-order polynomial actually interpolates the data points. From the figure, it is clear that the error in the extrapolated kernels grows quickly as the unstable flow velocity of 12.4 m/s is approached. The fifth-order polynomial provides the most accurate extrapolation. As a point of comparison, the error in the extrapolated kernels exceeds 10% at a flow velocity of about 9.5 m/s for the fifth-order fit. In contrast, the error exceeds 10% at $\{6.0, 7.5, 8.25, 9.0\}$ m/s for the linear, quadratic, cubic, and fourth-order fits, respectively. The differences in the errors in the curve-fits become less pronounced as the flow velocity increases. Then, the error becomes large regardless of the order of the polynomial fit.

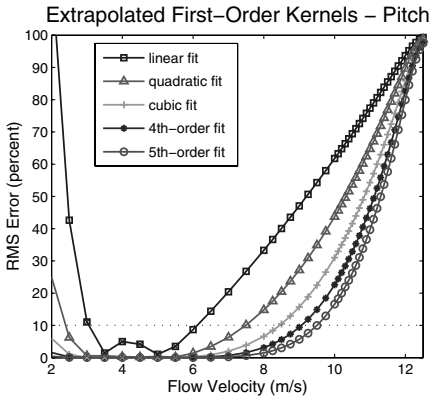

Fig. 2 RMS error in extrapolated pitch first-order kernels, linear through fifth-order polynomial models.

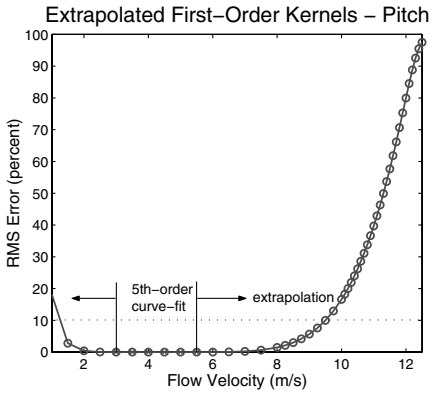

Fig. 3 RMS error in extrapolated pitch first-order kernels, fifth-order polynomial model.

In this case, a fifth-order fit is clearly more accurate than the lower-order polynomial models. Figure 3 shows the error in the extrapolated pitch kernels from the fifth-order fit alone. The circles denote the actual points where the kernels were extrapolated. Also, the points used in the curve-fit are clearly marked in the figure. The results show that for this curve-fit, where the last data point was at 5.5 m/s, kernels within an rms error tolerance of 10% can be extrapolated to flow velocities as large as 9.5 m/s. Unfortunately, the error grows rapidly beyond this point and the extrapolated kernels are unable to predict the approach of the instability. Kernels were also extrapolated in the direction of decreasing flow velocity. Once the velocity decreases below 1 m/s, the error exceeds 10% and grows very large. This is possibly due to the fact that the kernels are extremely small at such low velocities.

Figures 2 and 3 were generated for the pitch angle first-order kernels. Similar results were obtained for the plunge first-order kernels and have not been shown here. A number of the extrapolated kernels have been plotted in comparison to the true measured kernels. Figure 4 depicts the extrapolated pitch first-order kernels for flow velocities of $\{7, 8, 9, 10, 11, 12\}$ m/s. The increasing error as the flow velocity approaches the instability is evident in the plots. To provide a sense of the predictive ability of the extrapolated kernels, the predicted pitch responses to a linear chirp input, with a frequency range of 0–4 Hz, are shown in Fig. 5. The rms error in the predicted responses is plotted in Fig. 6.

Adaptive Curve-Fit and First-Order Kernel Extrapolation

This example attempts to simulate a possible application of the kernel extrapolation technique in the flight test environment. In this case, a curve-fit is first performed using a set of measured kernels. This model is used to extrapolate kernels at higher flow velocities until the error exceeds a chosen tolerance. At that point, a new kernel is measured from the data and a new curve-fit is performed that includes the newly measured kernel. Once again, kernels are extrapolated until the error tolerance is exceeded. The procedure continues, with new kernels being measured every time an extrapolated kernel violates the error criterion. In practice, this would be equivalent to adding a new flight test point every time the extrapolation error exceeds the chosen threshold.

In this example, an initial fifth-order curve-fit is performed from the pitch kernels measured at

$$U_{\text{fit}} = \{3.0, 3.5, 4.0, 4.5, 5.0, 5.5\} \text{ m/s}$$

the same set of velocities used in the preceding example. In this case, the error tolerance has been chosen as 10% rms error. Kernels are then extrapolated at increasing velocities. At $U = 9.75$ m/s, the rms error exceeds the 10% threshold, indicating the need to measure a new kernel. Therefore, the measured pitch kernel at 9.75 m/s is

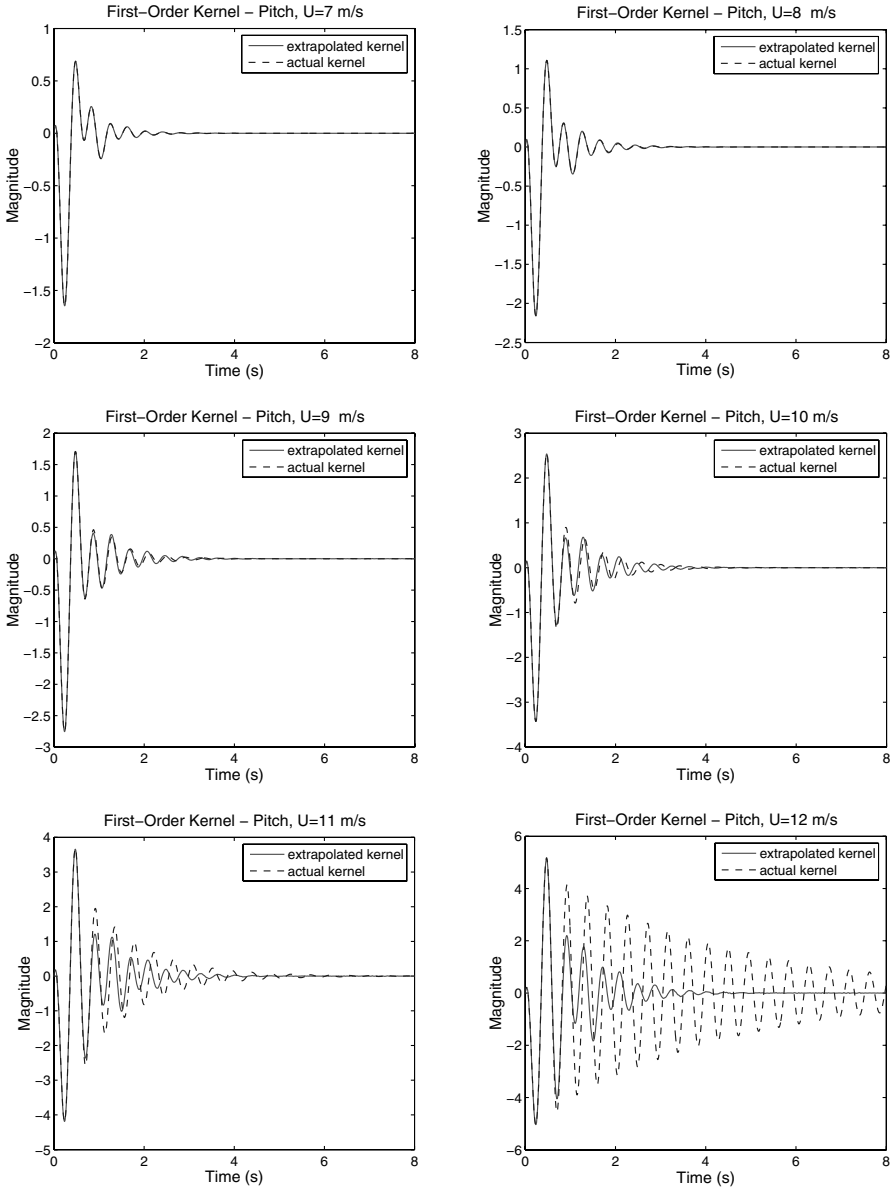

Fig. 4 Extrapolated pitch first-order kernels for flow velocities {7, 8, 9, 10, 11, 12} m/s.

included in a new curve-fit. At this point, one can choose to simply add the kernel from the new test point to the original set of six kernels and perform a new fifth-order curve-fit using all seven measured kernels. In contrast to this global curve-fit, one might choose a local fit using only the most recent six kernels (i.e., the 3 m/s kernel would no longer be included in the extrapolation model). Both options have been explored in this study. Another option, which was not implemented, is to perform a global fit and increase the degree of the polynomial each time. In this manner, the polynomial would interpolate all the data points. This is not expected to be a desirable option, however, when using kernels measured from noisy flight data. Such kernels can be anticipated to have a high degree of uncertainty. Therefore, interpolating all the measured kernels with increasingly higher-order polynomials would almost certainly not be an effective procedure.

Figure 7 shows the error in the extrapolated pitch kernels using a fifth-order global curve-fit and an error tolerance of 10%. The procedure required that new kernels be measured at {9.75, 10.6, 11.2, 11.6, 11.9, 12.0, 12.1, 12.2, 12.3, 12.4, 12.5} m/s. These points are indicated by the vertical lines in the plot, which shows that the kernel has been computed twice at these points. The drop in the error is due to recomputing the kernel using the new curve-fit. Basically, these results imply that the procedure is ineffective for extrapolating kernels beyond 11.9 m/s. After that point, every extrapolated kernel violates the error tolerance and the extrapolation has no predictive value.

Figure 8 illustrates the alternative approach whereby a local curve-fit is employed. Therefore, each time a new measured kernel is included in the curve-fit, only the most recent six measured kernels are used. As an example, after the initial curve-fit, the next curve-fit includes the measured kernels at {3.5, 4.0, 4.5, 5.0, 5.5, 9.75} m/s. As anticipated, the local fit has the benefit of adapting better to recent variations in the kernels. Using this approach for the extrapolated pitch kernels and the same error criterion, new kernels needed to be measured at {9.75, 10.6, 11.2, 11.7, 12.0, 12.2, 12.5} m/s. In this case, the procedure is able to effectively extrapolate kernels for very small steps in flow velocity as the instability approaches. Note that, although Figs. 7 and 8 refer to data points at 12.5 m/s, it would not be practical to measure flight data at speeds greater than the linear flutter speed of 12.4 m/s. Strictly speaking, the Volterra theory is no longer applicable to the system beyond this point because the Volterra series is valid only for systems with fading memory (i.e., the kernels need to decay to zero in finite time).

Similar results were obtained using the plunge first-order kernels and have not been shown here. This example shows the possible benefit of the kernel extrapolation procedure in a flight test environment. The error in the extrapolated kernels could be used as an indicator as to how large a step in velocity can safely be taken

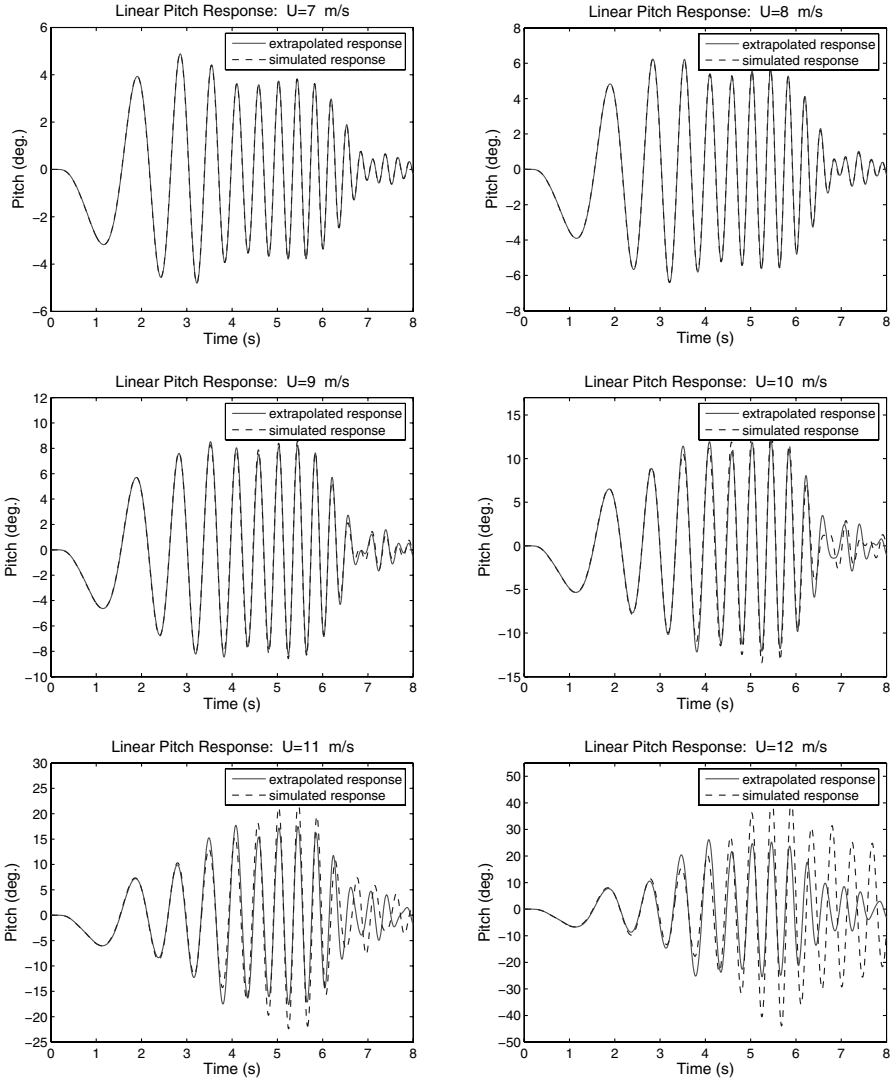

Fig. 5 Extrapolated pitch responses for flow velocities {7, 8, 9, 10, 11, 12} m/s.

before a new test point is needed. Obviously, in a flight test, one does not have access to the true kernels to compute error estimates. Instead, the error estimates would need to be in terms of uncertainty estimates on the measured kernels. The incorporation of such uncertainty estimates into the procedure is an important consideration for future work.

Second-Order Kernel Extrapolation

The second-order kernel extrapolation procedure is identical to the method used in the first-order case. That is, an extrapolation model is obtained by curve-fitting the two-dimensional basis coefficients that represent the second-order kernels. Second-order Volterra kernels were extracted from simulated data from the nonlinear pitch-plunge aeroelastic system described in Eq. (5). The kernels were identified using a 32 s random input with a sampling rate of 128 Hz. Each kernel was represented in terms of 153 basis functions over a 2 s time interval, corresponding to a rather coarse representation. For almost all values of the flow velocity, the kernels decay to zero within 2 s. As the flow velocity approaches the linear flutter point at 12.4 m/s, however, the kernels no longer decay to zero within that time interval. Unfortunately, as the flow velocity exceeded 11 m/s, the

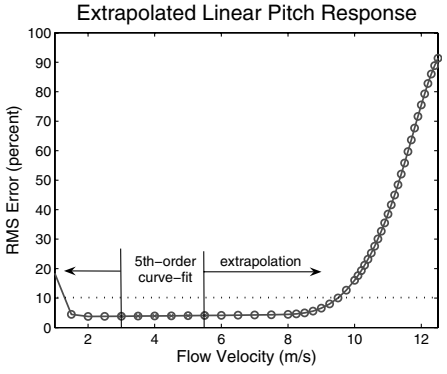

Fig. 6 RMS error in extrapolated pitch responses, fifth-order polynomial model.

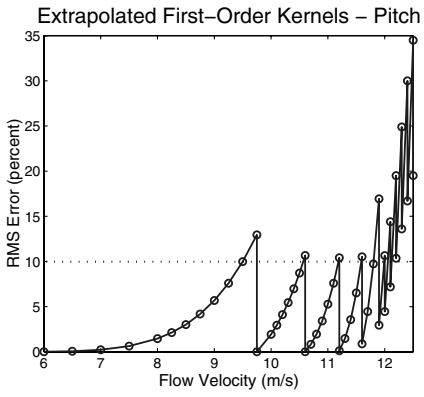

Fig. 7 RMS error in extrapolated pitch kernels, fifth-order global polynomial fit.

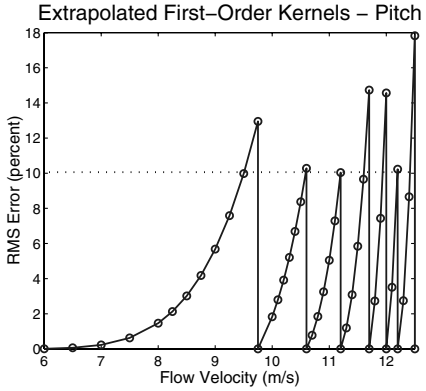

Fig. 8 RMS error in extrapolated pitch kernels, fifth-order local polynomial fit.

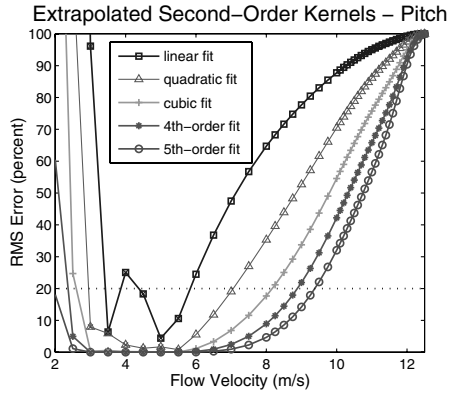

Fig. 9 RMS error in extrapolated pitch second-order kernels, linear through fifth-order polynomial models.

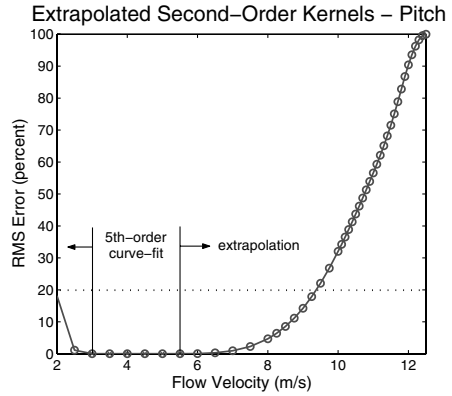

Fig. 10 RMS error in extrapolated pitch second-order kernels, fifth-order polynomial fit.

identified kernels became increasingly unreliable. Despite increasing the memory of these kernels, accurate results still were not obtained. This speaks to the difficulty in measuring higher-order kernels and may be due to the coarseness of the representation and problems with overfitting the data when the memory is increased.

It should be noted that, under the most general circumstances, the first- and second-order Volterra kernels need to be identified simultaneously from the data. In theory, however, the system output can be decomposed into contributions from the even-ordered kernels and the odd-ordered kernels. This can be accomplished using the measured response y to an input u and the measured response y_{neg} to the negative of the input $-u$. The even- and odd-ordered contributions can then be computed as

$$y_{\text{even}} = y + y_{\text{neg}} \qquad y_{\text{odd}} = y - y_{\text{neg}} \tag{8}$$

In this paper, a truncated Volterra model is used that includes only the first- and second-order kernels. Therefore, the odd-ordered response is modeled by the first-order kernel and the even-ordered response is modeled by the second-order kernel. Using the decomposition in Eq. (8) is a convenient means of approximating the contribution of the second-order kernel to the overall response. In this example, the second-order kernels have been identified from the signal y_{even}, which increases the accuracy of the identified kernels. It should be noted that the decomposition in Eq. (8) cannot usually be achieved in practice due to noise in the measured data. It has been used in this study to generate more accurate second-order kernel estimates for the purposes of evaluating the extrapolation procedure under ideal conditions.

Second-order kernels were extrapolated from polynomial models of the basis coefficients and compared with the actual identified kernels. An rms error for each extrapolated kernel is defined as

$$E_2 = \frac{\{\sum_{i=1}^{p_2}\sum_{j=1}^{p_2}[h_2(i,j) - \hat{h}_2(i,j)]^2\}^{1/2}}{\{\sum_{i=1}^{p_2}\sum_{j=1}^{p_2} h_2(i,j)^2\}^{1/2}} \tag{9}$$

where h_2 denotes the actual measured kernel and $\hat{h}_2$ represents the extrapolated kernel. Each kernel is plotted in terms of a square grid of discrete points ($p_2 = 129$), and these discrete kernel values are used to compute the rms error measure. Here it should be noted that, unlike the first-order case, the measured second-order kernels have a significant amount of error. This error is due to the coarseness of the kernel representations as well as possible contributions from even-ordered kernels of fourth-order and higher (i.e., truncation error).

As an example, consider the extrapolation of second-order pitch kernels using the kernels identified at the following six flow velocities:

$$U_{\text{fit}} = \{3.0, 3.5, 4.0, 4.5, 5.0, 5.5\} \text{ m/s}$$

Polynomial curve-fits are performed for each of the 153 basis coefficients as they vary across these six flow velocities. In this manner, each basis coefficient is modeled as a polynomial function of flow velocity. This model enables the prediction of the value of each

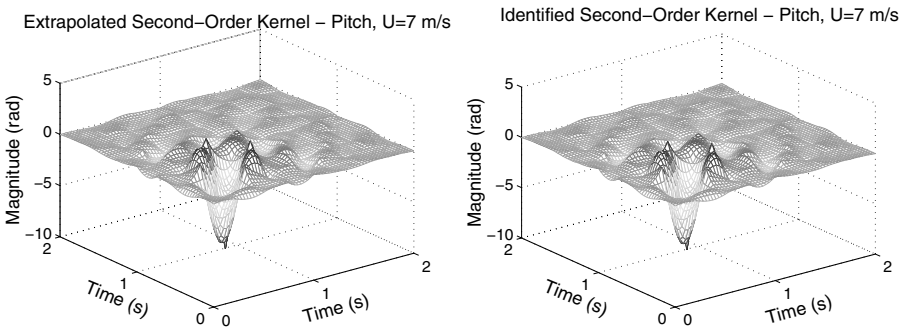

Fig. 11 Extrapolated and measured pitch second-order kernels, $U = 7$ m/s.

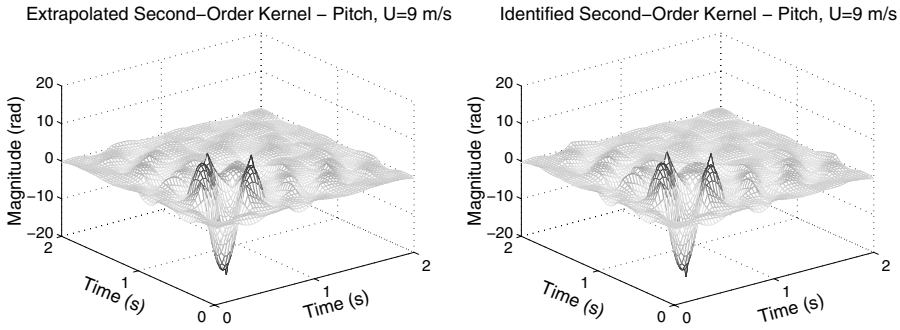

Fig. 12 Extrapolated and measured pitch second-order kernels, $U = 9$ m/s.

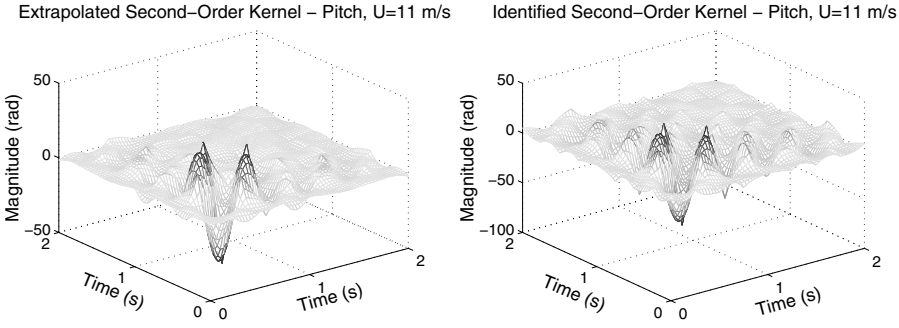

Fig. 13 Extrapolated and measured pitch second-order kernels, $U = 11$ m/s.

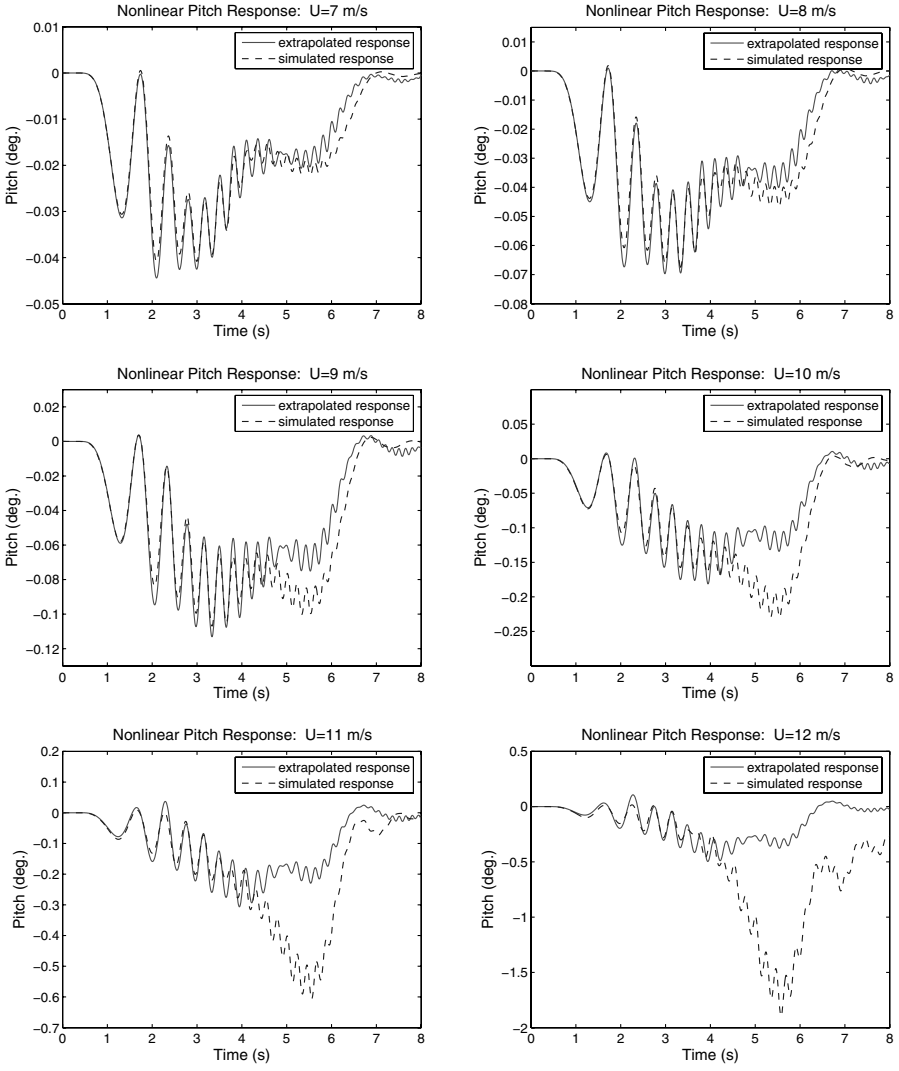

Fig. 14 Extrapolated nonlinear pitch response for flow velocities {7, 8, 9, 10, 11, 12} m/s.

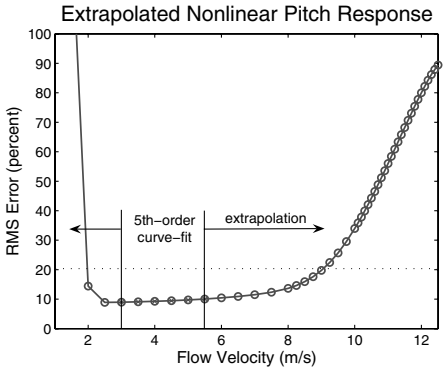

Fig. 15 RMS error in extrapolated nonlinear pitch response, fifth-order polynomial model.

basis coefficient at any given flow velocity and, consequently, yields an estimate of the second-order kernel.

Figure 9 plots the error in the extrapolated pitch kernels as a function of flow velocity for different polynomial fits. In this example, linear, quadratic, cubic, fourth-order, and fifth-order fits were performed. As in the first-order case, each polynomial model was obtained by solving a least-squares problem for each polynomial coefficient. From the figure, it is clear that the error in the extrapolated kernels grows quickly as the flow velocity approaches 12.4 m/s. In each case, the rms error approaches 100%. This is probably due to the fact that the measured kernels become quite large near the linear flutter speed whereas the extrapolated kernels do not. Therefore, the ratio in Eq. (9) approaches unity. For flow velocities exceeding 11 m/s, the measured kernels are increasingly unreliable, and, therefore, the results beyond 11 m/s in Fig. 9 are not accurate at all.

In any event, the fifth-order polynomial provides the most accurate extrapolation. As a point of comparison, the rms error in the extrapolated kernels exceeds 20% at a flow velocity of about 9.5 m/s for the fifth-order fit. In contrast, the error exceeds 20% at about $\{5.5, 7.0, 8.0, 9.0\}$ m/s for the linear, quadratic, cubic, and fourth-order fits, respectively. The differences in the errors in the curve-fits become less pronounced as the flow velocity increases. Then, the error is large regardless of the order of the polynomial fit.

In this case, a fifth-order fit clearly yields the best performance. Figure 10 shows the error in the extrapolated pitch kernels from the fifth-order fit alone. The circles denote the actual points where the

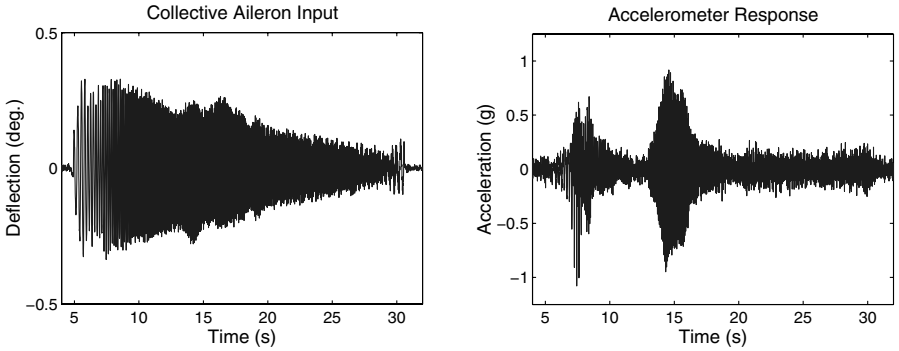

Fig. 16 Collective aileron input and accelerometer response at Mach 0.85, 15,000 ft.

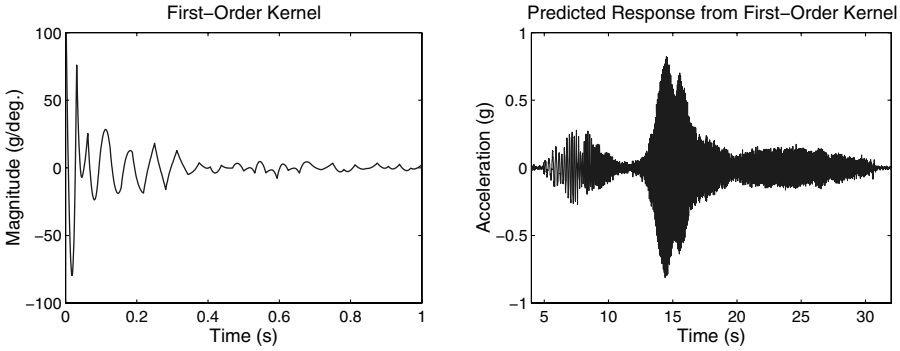

Fig. 17 Identified first-order kernel and predicted response, Mach 0.85 at 15,000 ft.

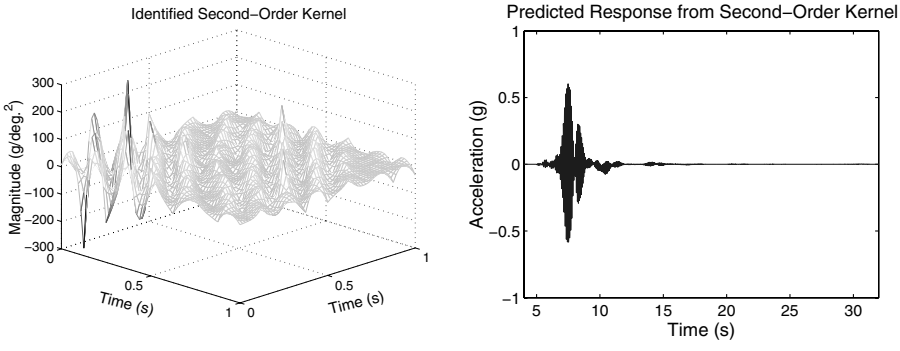

Fig. 18 Identified second-order kernel and predicted response, Mach 0.85 at 15,000 ft.

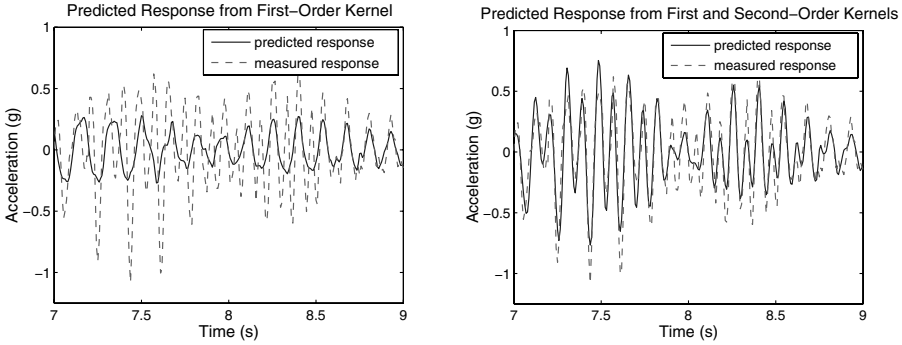

Fig. 19 Predicted responses using the first-order kernel and the total Volterra model: Mach 0.85 at 15,000 ft.

kernels were extrapolated. Also, the points used in the curve-fit are clearly marked in the figure. The results show that for this curve-fit, where the last data point was at 5.5 m/s, kernels within an error tolerance of 20% can be extrapolated out to about 9.5 m/s. Unfortunately, as in the first-order case, the error grows rapidly beyond this point, and the extrapolated kernels are unable to predict the approach of the linear flutter point. Kernels were also extrapolated in the direction of decreasing flow velocity. Once the velocity decreases below 2 m/s, the error exceeds 20% and grows very large. This is possibly due to the fact that the kernels are very small at such low velocities.

Finally, some of the extrapolated second-order kernels have been plotted in comparison to the true measured kernels. Figures 11–13 depict the extrapolated pitch kernels for flow velocities of 7, 9, and 11 m/s. The increasing extrapolation error as the flow velocity approaches the linear flutter speed is evident in the figures. The predicted responses of the extrapolated second-order kernels to a linear chirp excitation (0–4 Hz frequency range) are shown in Fig. 14. In each case, the predicted response is compared with the signal y_{even} defined in Eq. (8). Figure 15 depicts the rms error in the predicted responses.

Flight Data Analysis: F/A-18 Active Aeroelastic Wing

The examples given in the preceding section serve to demonstrate the validity of the kernel extrapolation method and also illustrate

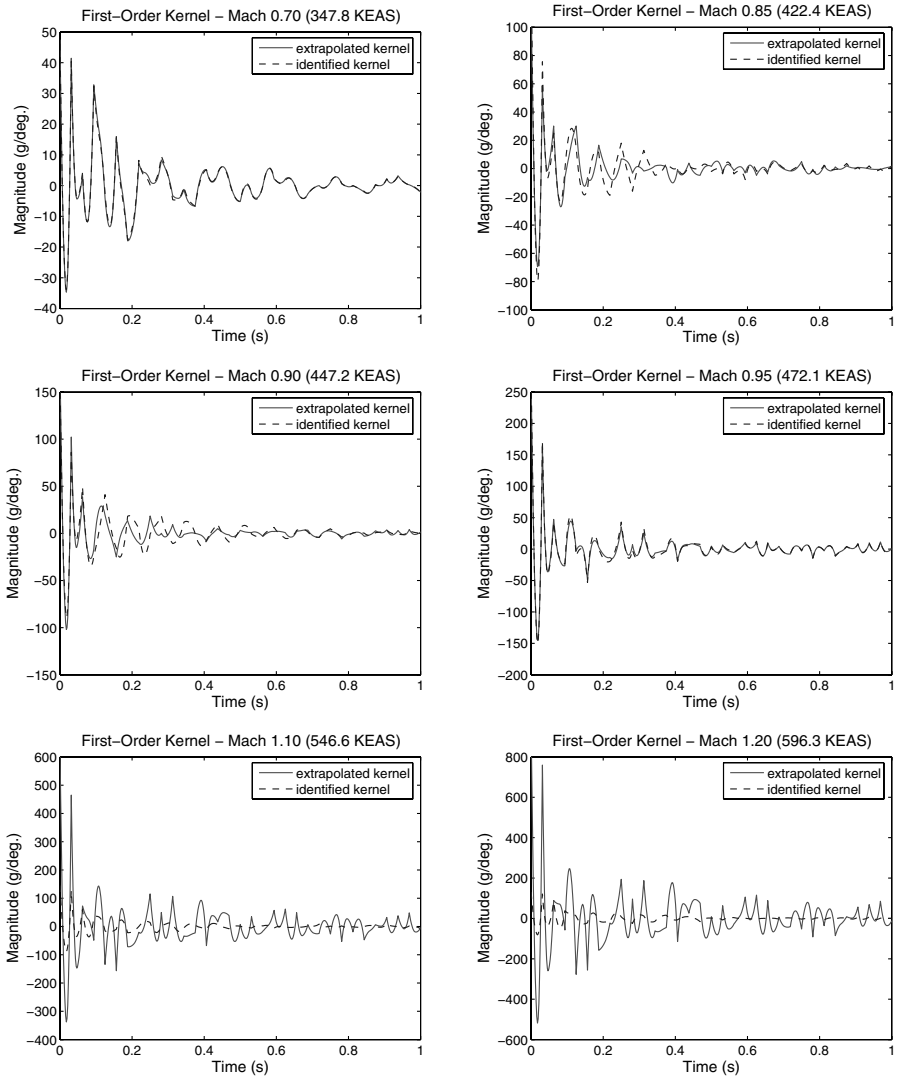

Fig. 20 Extrapolated first-order kernels at 15,000 ft for varying Mach numbers.

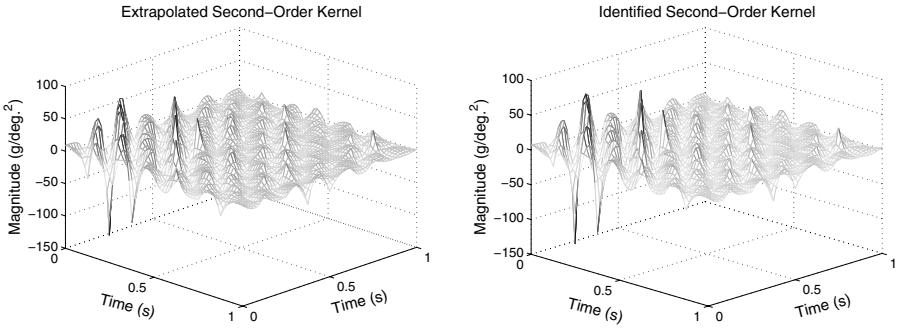

Fig. 21 Extrapolated and measured second-order kernels at Mach 0.70, 15,000 ft.

some of the limitations. In particular, and as expected, the accuracy of the extrapolated kernels degrades with increasing distance from the test points used for the extrapolation model curve-fit. This section discusses the feasibility of the extrapolation of first- and second-order kernels from flight data from the F/A-18 Active Aeroelastic Wing (AAW).

Flight testing of the AAW began in November of 2002 at the NASA Dryden Flight Research Center. The AAW employs technology whereby wing aeroelastic flexibility is used to control the aircraft [28]. The main objective of this control strategy is to eliminate the problem of aileron reversal at high dynamic pressures by using wing twist for control instead of trailing-edge surfaces. The controlled wing twist is actuated through the use of multiple leading and trailing-edge control surfaces activated by a digital flight control system. Using energy from the airstream, the necessary wing twist can be generated with minimal control surface deflections. The AAW employs more control surfaces than the standard F/A-18 and operates at high-subsonic, transonic, and low-supersonic flight conditions. Therefore, it has the potential to exhibit significant nonlinear behavior. This underscores the need for models that can account for nonlinear aeroelastic effects.

During the AAW flutter clearance flights, data were collected over a wide range of flight conditions. At each flight condition, the aircraft was subjected to multisine inputs corresponding to collective and differential aileron, collective and differential leading-edge flap, rudder, and collective stabilator excitations in the range of 3–35 Hz. This paper focuses on the Volterra kernels that model a particular single-input/single-output subsystem of the AAW over a range of flight conditions. The input is taken as the collective aileron position, obtained as the average of four position transducer measurements from the right and left ailerons during the sweep. The output is taken as the response of an accelerometer mounted towards the front of the right wing, just inside the wing fold.

As an example, the collective aileron input and corresponding accelerometer response measured at a flight condition of Mach 0.85 at 15,000 ft are shown in Fig. 16. Both signals have been resampled at 256 Hz for ease of computation. In addition, they have been high-pass filtered at 2 Hz to remove the lowest-frequency dynamics and the means of the signals. First- and second-order kernels were identified from these flight data and are depicted in Figs. 17 and 18. Also shown in the figures are the responses predicted by these identified kernels. Of particular interest is the fact that, whereas the linear model captures most of the response, it is unable to characterize the dynamics in the 7–9 s time interval. The second-order kernel, however, is able to predict much of the nonlinear dynamic response in this time range. This is demonstrated in Fig. 19 which, for the 7–9 s time interval, shows the responses predicted by the first-order kernel alone and the total model consisting of both the first- and second-order kernels. Clearly, the inclusion of the second-order kernel in the model leads to a more accurate prediction.

First- and second-order kernels were extracted from the flight data over a range of flight conditions. In general, the flight conditions are a function of two varying parameters, such as Mach number and altitude. The extrapolation technique explored in this paper has been designed for a single varying parameter. Therefore, it is desirable to consider the AAW kernels as a function of only a single parameter. One option is to approximate each flight condition in terms of knots of equivalent airspeed (KEAS). This approximation is valid for subsonic flight conditions, but becomes less accurate at transonic and supersonic conditions where compressibility effects are more significant. In this example, the evolution of the first- and second-order kernels as a function of Mach number at a fixed altitude of 15,000 ft is considered. It was not feasible to extrapolate the kernels as a function of varying altitude because, for any given Mach number, flight data were taken at no more than three different altitudes. As will be shown, there are some difficulties associated with extrapolating kernels at varying Mach numbers because the aerodynamics change considerably across subsonic, transonic, and supersonic flight conditions. Still, this study provides enough useful data to obtain a qualitative assessment of the extrapolation strategy.

Specifically, flight data were collected at 15,000 ft at Mach numbers $\{0.50, 0.70, 0.85, 0.90, 0.95, 1.10, 1.20\}$. Each identified first-order kernel is represented in terms of 112 multiwavelet coefficients and a memory of 2 s. Each second-order kernel is represented in terms of 153 unique basis coefficients and a memory of 1 s. In this example, the kernels identified at Mach numbers $\{0.70, 0.85, 0.90, 0.95\}$ were used for the extrapolation model, which employed a quadratic curve-fit for the basis coefficients. Higher-order curve-fits generally yielded worse results due to the fact that the kernels are relatively noisy, a consequence of noise in the original flight data. It should be emphasized that, unlike the analytical study, the first- and second-order kernels were identified simultaneously from the same input/output data.

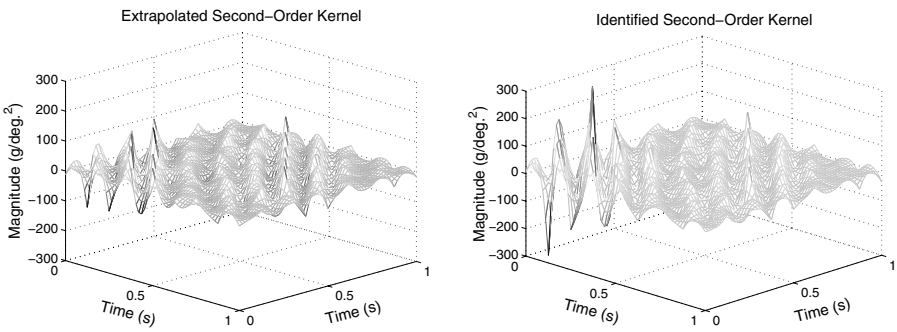

Fig. 22 Extrapolated and measured second-order kernels at Mach 0.85, 15,000 ft.

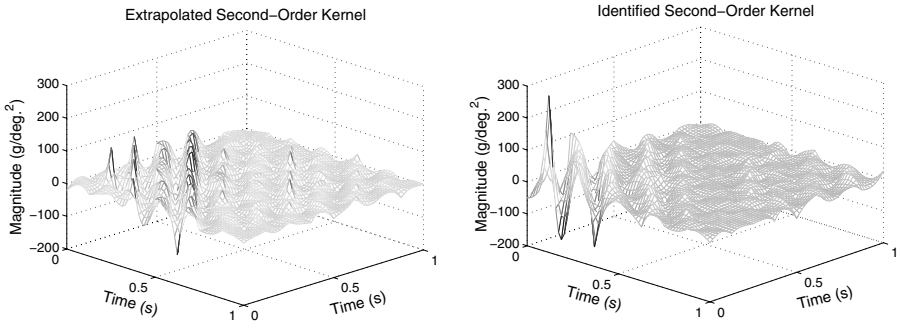

Fig. 23 Extrapolated and measured second-order kernels at Mach 0.90, 15,000 ft.

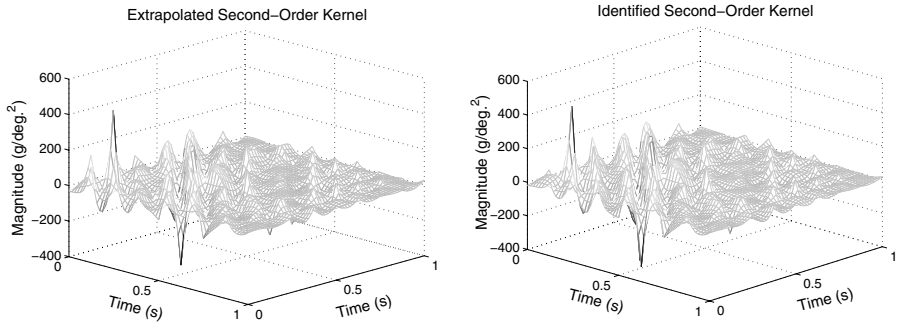

Fig. 24 Extrapolated and measured second-order kernels at Mach 0.95, 15,000 ft.

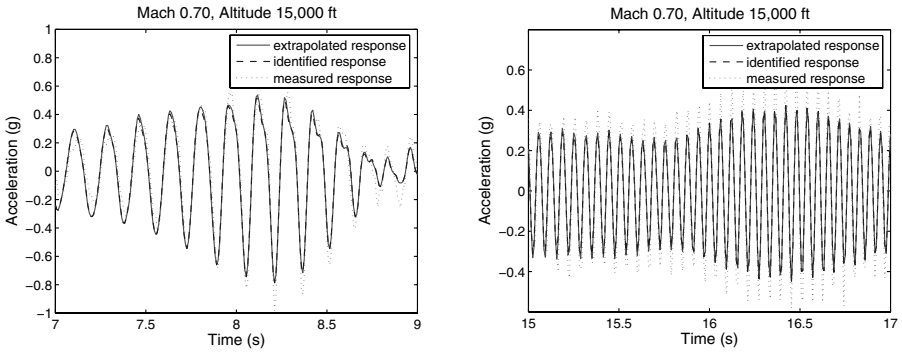

Fig. 25 Extrapolated acceleration response at Mach 0.70, 15,000 ft.

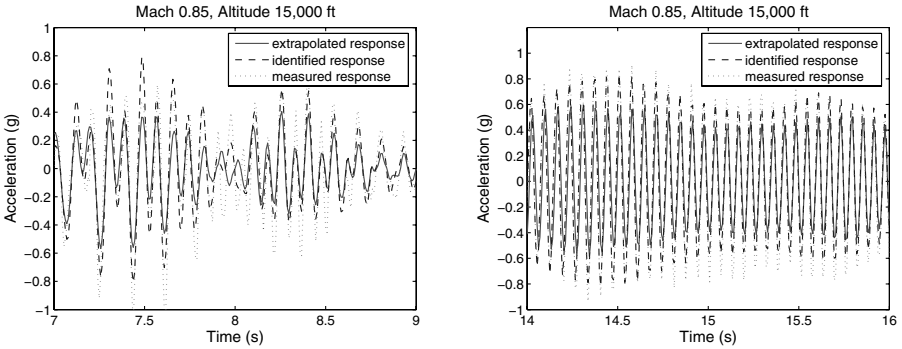

Fig. 26 Extrapolated acceleration response at Mach 0.85, 15,000 ft.

Some of the extrapolated first-order kernels are depicted in Fig. 20 and compared with the identified kernels. The results show that qualitatively reasonable estimates of the kernels used to form the extrapolation model are obtained. Unlike the analytical case studied earlier, this is not a trivial result owing to the fact that the kernels are noisy and a low-order curve-fit was employed. The results also show that, in this case, it is not feasible to extrapolate first-order kernels into the supersonic flight regime. This is most likely due to fundamental changes in the aerodynamics from the transonic to supersonic flight regimes. Some of the extrapolated second-order kernels are compared with the identified kernels in Figs. 21–24. Similar to the first-order kernels, it is not feasible to extrapolate the second-order kernels into supersonic flight conditions.

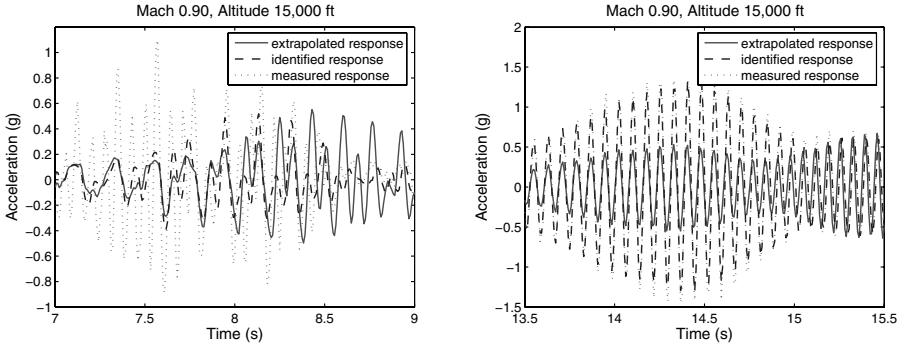

Fig. 27 Extrapolated acceleration response at Mach 0.90, 15,000 ft.

The predicted responses using the extrapolated kernels are depicted in Figs. 25–29. These plots show the acceleration predicted by the extrapolated kernels, the acceleration predicted by the identified kernels, and the measured acceleration. In the figures, the extrapolated responses represent the total combined responses from the extrapolated first- and second-order kernels. In each case, the plots focus on two regions of the data: a "nonlinear region" where significant nonlinear response occurs at several flight conditions and a "linear region" where a mode of vibration has been excited. The region of nonlinear response corresponds to the response of the system to 6–7 Hz excitation whereas the linear region corresponds to roughly 14 Hz excitation. Note that, due to differences in the starting time of the input excitation at each flight test point, these regions occur over different time ranges in the data sets. For the test points used in the extrapolation model, the extrapolated kernels provide a reasonable approximation of the response in the linear region, which is dominated by the first-order kernel. At Mach number 0.90, however, the extrapolated response is severely underpredicted in the linear region. At Mach 1.10, the extrapolated response is severely overpredicted in the linear region.

The system behavior in the nonlinear region varies significantly with the Mach number. At Mach numbers 0.70 and 0.95, the response in this region appears to be nearly linear and is well approximated by the extrapolated first-order kernels. At Mach number 0.85, the nonlinear region appears to be characterized by a quadratic nonlinearity which is partially captured by the extrapolated second-order kernel. At Mach number 0.90, the response in this region is clearly nonlinear because the response frequency is much higher than the input frequency. The extrapolated second-order kernel, and the identified second-order kernel for that matter, fail to capture most of this nonlinear response. This implies that higher-order kernels may be necessary to model the nonlinearity at this flight condition. At Mach number 1.10, there is very little response in this region, implying that in the supersonic flight regime, there is no significant nonlinearity in this region. The variation of this system nonlinearity with Mach number is a topic that is explored in more detail in a companion paper that considers the identification of first-, second-, and third-order Volterra kernels from flight data [29].

Conclusions

This paper has presented a simple approach for Volterra kernel extrapolation in which the kernel basis coefficients are modeled as polynomial functions of a single varying parameter. Such an approach is applicable as long as the kernels are represented in terms of a set of basis functions. In particular, the kernels in this paper have been identified from measured input/output data using a multiwavelet-based algorithm. The extrapolation procedure has

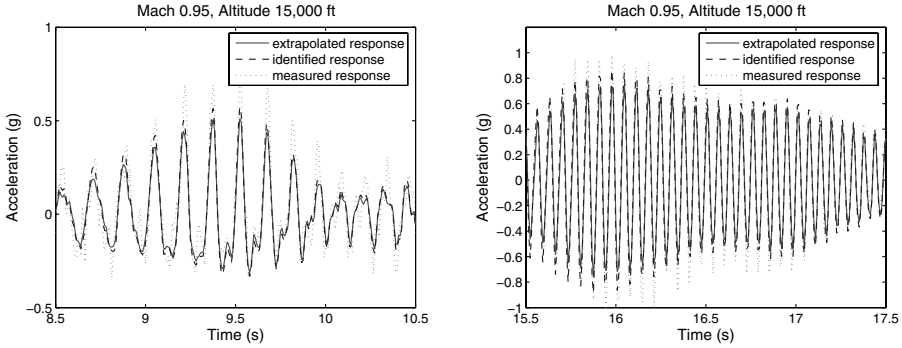

Fig. 28 Extrapolated acceleration response at Mach 0.95, 15,000 ft.

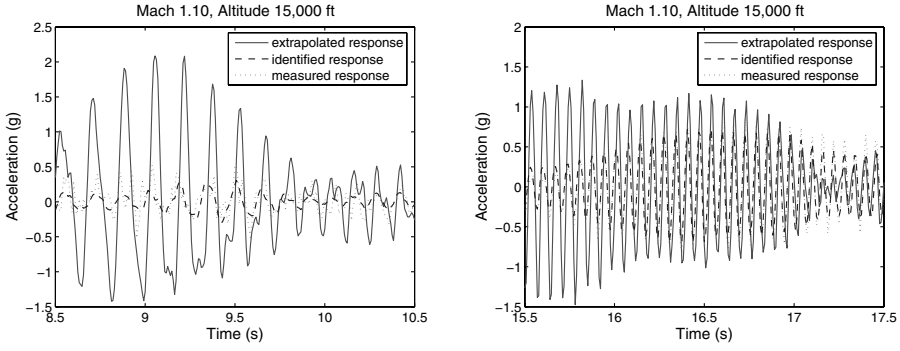

Fig. 29 Extrapolated acceleration response at Mach 1.10, 15,000 ft.

been validated using data from a simulated pitch-plunge aeroelastic system. In that example, it was shown that first- and second-order kernels can effectively be extrapolated over a range of flow velocities. As expected, the accuracy of the extrapolation deteriorates as the kernels are extrapolated further from the velocities used in the model. The effective range of extrapolation becomes smaller as the linear flutter speed is approached, reflecting the fact that the system changes more rapidly near the flutter point.

The feasibility of applying this kernel extrapolation method to flight data from the F/A-18 Active Aeroelastic Wing has also been investigated. In particular, an extrapolation model was formed to express the kernels measured at a constant altitude as a function of varying Mach number. Because of significant noise in the flight data, a quadratic polynomial fit was used in the extrapolation model. The model provided reasonably accurate estimates of the first- and second-order kernels at the subsonic and transonic test points used to form the extrapolation model. It was also observed that the kernels could not be extrapolated into the supersonic flight regime, most likely due to fundamental changes in the aerodynamics as the Mach number varies. These experimental results illustrate the difficulty in extrapolating kernels from noisy flight data. This paper only considered a small subset of data and further study is certainly required. It should be noted that better extrapolation results might be obtained using globally supported basis functions such as Laguerre polynomials, which could yield smoother kernel estimates. Using such functions generally results in a less efficient kernel identification algorithm, however. Finally, another topic for future research would be to extrapolate Volterra kernels in terms of two varying parameters. In this case, the kernel basis coefficients would be curve-fit using two-dimensional functions. This extension would enable the extrapolation of AAW kernels as functions of both altitude and Mach number.

Acknowledgments

The research presented in this paper was performed by the University of Florida and Nielsen Engineering and Research, Inc., as part of an STTR supported by the NASA Dryden Flight Research Center, contract number NASA-03012. The authors would like to thank the anonymous reviewers for many helpful suggestions for improving this paper.

References

[1] Dowell, E., Edwards, J., and Strganac, T., "Nonlinear Aeroelasticity," *Journal of Aircraft*, Vol. 40, No. 5, Sept.–Oct. 2003, pp. 857–874.

[2] Lee, B., Price, S., and Wong, Y., "Nonlinear Aeroelastic Analysis of Airfoils: Bifurcation and Chaos," *Progress in Aerospace Sciences*, Vol. 35, No. 3, April 1999, pp. 205–339.

[3] Baldelli, D., Lind, R., and Brenner, M., "Robust Aeroelastic Match-Point Solutions Using Describing Function Method," *Journal of Aircraft*, Vol. 42, No. 6, Nov.–Dec. 2005, pp. 1597–1605.

[4] Silva, W., and Dunn, S., "Higher-Order Spectral Analysis of F-18 Flight Flutter Data," AIAA Paper 2005-2014, April 2005.

[5] Silva, W., Strganac, T., and Hajj, M., "Higher-Order Spectral Analysis of a Nonlinear Pitch and Plunge Apparatus," AIAA Paper 2005-2013, April 2005.

[6] Denegri, C., and Johnson, M., "Limit Cycle Oscillation Prediction Using Artificial Neural Networks," *Journal of Guidance, Control, and Dynamics*, Vol. 24, No. 5, Sept.–Oct. 2001, pp. 887–895.

[7] Liu, L., and Dowell, E., "Harmonic Balance Approach for an Airfoil with a Freeplay Control Surface," *AIAA Journal*, Vol. 43, No. 4, April 2005, pp. 805–815.

[8] Kukreja, S., and Brenner, M., "Nonlinear Aeroelastic System Identification with Application to Experimental Data," *Journal of Guidance, Control, and Dynamics*, Vol. 29, No. 2, March–April 2006, pp. 374–381.

[9] Richards, C., Brenner, M., and Singh, R., "Identification of a Nonlinear Aeroelastic Aircraft Wing Model," AIAA Paper 2004-1941, April 2004.

[10] Brenner, M., and Prazenica, R., "Aeroelastic Flight Data Analysis Using the Hilbert-Huang Algorithm," AIAA Paper 2005-5917, Aug. 2005.

[11] Silva, W., "Application of Nonlinear Systems Theory to Transonic Unsteady Aerodynamic Responses," *Journal of Aircraft*, Vol. 30, No. 5, Sept.–Oct. 1993, pp. 660–668.

[12] Silva, W., "Discrete-Time Linear and Nonlinear Aerodynamic Impulse Responses for Efficient CFD Analyses," Ph.D. Dissertation, The College of William & Mary, Williamsburg, VA, 1997.

[13] Marzocca, P., Librescu, L., and Silva, W., "Aeroelastic Response of Nonlinear Wing Sections Using a Functional Series Technique," *AIAA Journal*, Vol. 40, No. 5, May 2002, pp. 813–822.

[14] Reisenthel, P., "Prediction of Unsteady Aerodynamic Forces via Nonlinear Kernel Identification," Nielsen Engineering and Research, Inc. Paper 379, June 1999.

[15] Prazenica, R., Brenner, M., and Lind, R., "Nonlinear Volterra Kernel Identification for the F/A-18 Active Aeroelastic Wing," IFASD Paper US-32, June 2003.

[16] Lind, R., Prazenica, R., and Brenner, M., "Estimating Nonlinearity Using Volterra Kernels in Feedback with Linear Models," *Nonlinear Dynamics*, Vol. 39, No. 1, Jan. 2005, pp. 3–23.

[17] Silva, W., "Identification of Nonlinear Aeroelastic Systems Based on the Volterra Theory: Progress and Opportunities," *Nonlinear Dynamics*, Vol. 39, No. 1, Jan. 2005, pp. 25–62.

[18] Lind, R., Prazenica, R., Brenner, M., and Baldelli, D., "Identifying Parameter-Dependent Volterra Kernels to Predict Aeroelastic Instabilities," *AIAA Journal*, Vol. 43, No. 12, Dec. 2005, pp. 2496–2502.

[19] Prazenica, R., and Kurdila, A., "Multiwavelet Constructions and Volterra Kernel Identification," *Nonlinear Dynamics*, Vol. 43, No. 3, Feb. 2006, pp. 277–310.

[20] Rugh, W., *Nonlinear System Theory: The Volterra-Wiener Approach*, Johns Hopkins Univ. Press, Baltimore, MD, 1980.

[21] Schetzen, M., *The Volterra and Wiener Theories of Nonlinear Systems*, John Wiley & Sons, New York, 1980.

[22] Boyd, S., Tang, Y., and Chua, L., "Measuring Volterra Kernels," *IEEE Transactions on Circuits and Systems*, Vol. CAS-30, No. 8, Nov. 1983, pp. 571–577.

[23] Raveh, D., Levy, Y., and Karpel, M., "Efficient Aeroelastic Analysis Using Computational Unsteady Aerodynamics," *Journal of Aircraft*, Vol. 38, No. 3, May–June 2000, pp. 547–556.

[24] Lee, Y., and Schetzen, M., "Measuring of the Wiener Kernels of a Non-Linear System by Cross-Correlation," *International Journal of Control*, Vol. 2, No. 3, 1965, pp. 237–254.

[25] Marmarelis, V., "Identification of Nonlinear Biological Systems Using Laguerre Expansions of Kernels," *Annals of Biomedical Engineering*, Vol. 21, No. 6, Nov. 1993, pp. 573–589.

[26] Mallat, S., *A Wavelet Tour of Signal Processing*, Academic Press, Boston, 1998.

[27] Donovan, G., Geronimo, J., and Hardin, D., "Intertwining Multiresolution Analyses and the Construction of Piecewise-Polynomial Wavelets," *SIAM Journal on Mathematical Analysis*, Vol. 27, No. 6, Nov. 1996, pp. 1791–1815.

[28] Pendleton, E., Bessette, D., Field, P., Miller, G., and Griffin, K., "Active Aeroelastic Wing Flight Research Program: Technical Program and Model Analytical Development," *Journal of Aircraft*, Vol. 37, No. 4, July–Aug. 2000, pp. 554–561.

[29] Prazenica, R., Brenner, M., Kurdila, A., and Lind, R., "Volterra Kernel Identification for Nonlinear Aeroelastic Systems," *Journal of Guidance, Control, and Dynamics*, (in review).